Performance of a MEMS Heat Exchanger for a Cryosurgical Probe

M.J. White[1], W. Zhu[2], G.F. Nellis[1], S.A. Klein[1], Y.B. Gianchandani[2]

[1]University of Wisconsin-Madison
[2]University of Michigan-Ann Arbor

ABSTRACT

This paper presents the experimental test results for two 2nd generation Micro-Electro-Mechanical Systems (MEMS) heat exchangers that are a composite of silicon plates with micro-machined flow passages interleaved with glass spacers. The MEMS heat exchangers were designed for use as the recuperative heat exchanger within a Joule-Thomson (JT) cycle used to energize a cryosurgical probe.

The heat exchangers were tested using two different methods. The first method utilized a cryocooler to provide the cooling at the cold end of the heat exchanger. This method allows a large temperature difference to be applied to the heat exchanger with a minimal pressure difference between the streams, and therefore allows accurate testing with little risk of failure. The second test method installs the heat exchanger in a JT cycle using either a micro-valve or orifice to create the isenthalpic pressure drop. A numerical model that includes estimated heat leaks was used to predict heat exchanger performance. The results of the numerical model are compared with experimental test results over a range of conditions. The second MEMS heat exchanger was fabricated with integrated platinum resistance thermometers (PRTs). Therefore, test results include spatially resolved internal temperature distributions, allowing detailed comparisons with the numerical model.

INTRODUCTION

Cryosurgery is a medical procedure in which malignant tissue such as cancer is destroyed by rapid freezing.[1] The procedure involves cooling the cells to a temperature below -50°C in repeated freeze/thaw cycles in order to ensure that all of the malignant tissue has been destroyed. The benefit of cryosurgery over other cancer treatment options is that tissue damage is localized and blood loss is minimal.

Conventional cryosurgical probes typically operate on a JT cycle.[2] A coiled finned tube wound around a small mandrel is generally used for the recuperative heat exchanger, and a fixed orifice is used to provide the isenthalpic expansion required for the cycle. The size of the metallic finned tube heat exchangers cannot easily be reduced further. Another drawback to conventional cryosurgical probes is the fixed orifice size. The integration of an actively controlled micro-valve would allow the effective orifice size to be adjusted to optimize the cycle for different cold end temperature and heat load requirements. In addition, the need for a heater during the thaw portion of the cycle could be eliminated if the valve was capable of opening

Cryocoolers 15, edited by S.D. Miller and R.G. Ross, Jr.

enough that there was minimal fluid expansion across the valve. The probe tip would quickly heat up due to the drop in cooling power and the flow of heat would be reversed so that heat is transferred the probe tip to the frozen lesion.

The goal of this project is to improve the design of cryosurgical probes through the use of MEMS-based technology. A first attempt at building a MEMS-based heat exchanger was unsuccessful.[3,4] These 1st-generation heat exchangers were fragile and broke frequently through handling or with small pressure differences. The 2nd-generation heat exchanger was entirely redesigned to address the deficiencies of the 1st-generation heat exchanger.[3] The 2nd-generation heat exchanger utilizes a perforated plate configuration. Initial experimental results were reported for the first prototype 2nd-generation heat exchanger[5,6] that included only a few plates. The focus of this paper is on the experimental testing of the most recent 2nd-generation heat exchanger that includes many more plates as well as integrated PRTs. The experimental data are compared to the results predicted by a numerical model.[7]

HEAT EXCHANGER GEOMETRY

The design of a 2nd-generation heat exchanger had several objectives. The heat exchanger must be lightweight and compact so that the probe can be easily held in the surgeon's hand. MRI-compatibility is a potential benefit since one current drawback to cryosurgery is that the surgeon can only estimate the size and location of the iceball formed at the probe tip using ultrasound. An MRI machine could be used to provide more accurate, real-time feedback to the surgeon regarding the status of the iceball.

Silicon and borosilicate glass, which are common MEMS materials, are used to fabricate the heat exchanger. The materials were selected in order to take advantage of existing MEMS processes and equipment which are compatible with these materials. MEMS device fabrication typically involves repeated masking and etching steps. Etching processes are effective for creating holes or trenches on a flat surface. However, creating large or complicated 3-D structures can be quite difficult using standard MEMS technology. Multiple perforated plates can be etched simultaneously on a single silicon wafer using a single masking and etching step. Instead of trying to fabricate the heat exchanger as a single complicated component, the heat exchanger is fabricated by making a large number of perforated plates and spacers and bonding them together. A simplified geometric model and a photograph of the 2nd-generation heat exchanger are shown in Fig. 1.

The two different types of dies that were fabricated in order to manufacture the 2nd-generation heat exchangers are shown in Fig. 2. The standard die, which is shown on the left, consists of one silicon perforated plate bonded to one glass spacer. Each die has outer dimensions of 10 mm by 10 mm and has a thickness of 0.8 mm (0.5 mm for the silicon plate and 0.3 mm for glass spacer). For each fluid stream there are two columns of 74 flow passages, with each flow passage having a length of 1.4 mm and thickness of 0.05 mm. The material that separates each duct has a thickness 0.05 mm. The integrated PRT die, which is shown to the

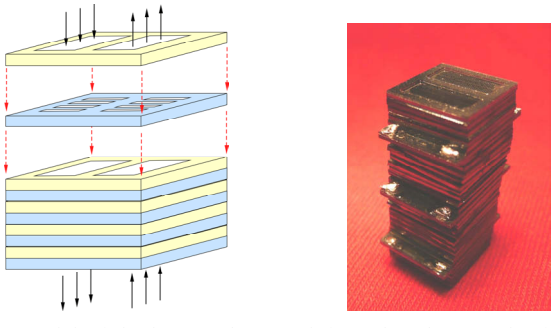

Figure 1. Geometric model of the heat exchanger (left) and a photograph of a heat exchanger before bonding with the headers (right).

Figure 2. Standard die consisting of one silicon perforated plate and one glass spacer (left) and a die that includes integrated PRTs (right).

right, is identical to the standard die except for the platinum wires that have been deposited onto the silicon surface. The integrated PRT dies are slightly wider so that measurement leads can be soldered to the platinum wire contacts.

The first heat exchanger that was tested is the 16-die heat exchanger shown in Fig. 3. The heat exchanger is fabricated by epoxying individual dies together in order to form a stack. The heat exchanger stack is epoxied to the G10 headers, and bolts are used to compress the heat exchanger to help prevent internal leakage and also to resist expansion of the heat exchanger due to internal pressurization. The G10 headers have large plenums so that the fluid flow will be evenly distributed before entering the heat exchanger, an important consideration for such a short heat exchanger. The outside of the heat exchanger is covered with a layer of epoxy to prevent external leakage.

A second, longer heat exchanger was subsequently constructed that included 43 dies, as shown in Fig. 4. The manufacturing process is identical to the 16-die heat exchanger. The second heat exchanger incorporated a number of integrated PRT dies so that the internal temperature distribution of the heat exchanger could be measured. Since the length of the second heat exchanger was much greater than the first, there was less concern about flow maldistribution, and therefore smaller stainless steel headers were used in order to reduce the thermal mass of the heat exchanger.

HEAT EXCHANGER TEST FACILITY

A flow schematic of the facility that is used to test the heat exchangers is shown in Fig. 5. The test facility is capable of testing the heat exchanger in two different modes of operation. The applied cooling mode uses a cryocooler to cool the fluid leaving the high-pressure side of the heat exchanger before it returns to the low-pressure inlet. This mode of testing allows large temperature differences to be applied to the heat exchanger while requiring only small pressure differences. The applied cooling tests were carried out first in order to ensure that high accuracy heat transfer data are collected without exposing it to large pressure differences, and therefore risking failure.

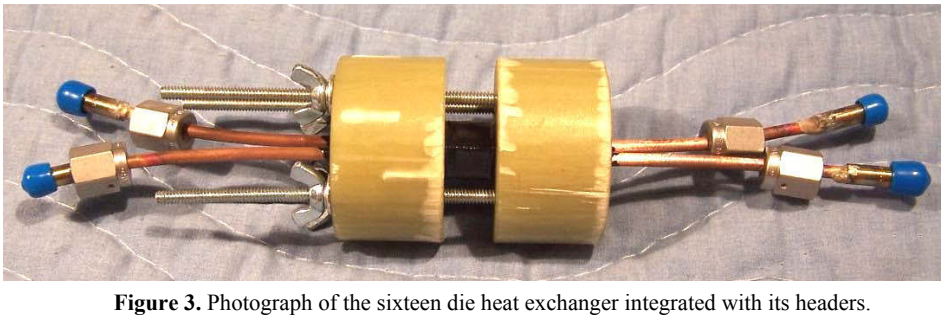

Figure 3. Photograph of the sixteen die heat exchanger integrated with its headers.

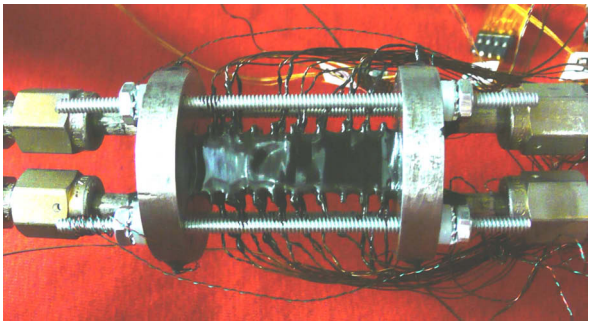

Figure 4. Photograph of the forty-three die heat exchanger integrated with its headers.

The second mode of testing involves self-cooling through the use of a JT cycle. An isenthalpic pressure drop, and therefore temperature drop, is created by placing either a precision jewel orifice or a valve between the high pressure outlet and the low pressure inlet. For the self-cooling tests, the tubing connections to the cryocooler heat exchanger are removed so that all flow is forced to pass through the valve or orifice. The temperature span produced across the heat exchanger for the self-cooling tests is much smaller than the applied cooling tests due to limitations of the JT cycle, and therefore the heat exchanger effectiveness measurements are less accurate. Also, the self-cooling tests inherently expose the heat exchanger to large pressure differences.

Two temperature sensors are inserted directly into the flowing fluid at each inlet and outlet of the heat exchanger. The first sensor is a commercially calibrated PRT, and the second sensor is a type-E thermocouple. The two temperature sensors were in excellent agreement, and the performance measurements associated with either sensor agreed nearly exactly. In addition, each inlet and outlet of the heat exchanger had a pressure tap, which was connected as shown in Fig. 5, in order to accurately measure both the absolute and differential pressures. A geometric model of the instrumentation assembly is shown in Fig. 6.

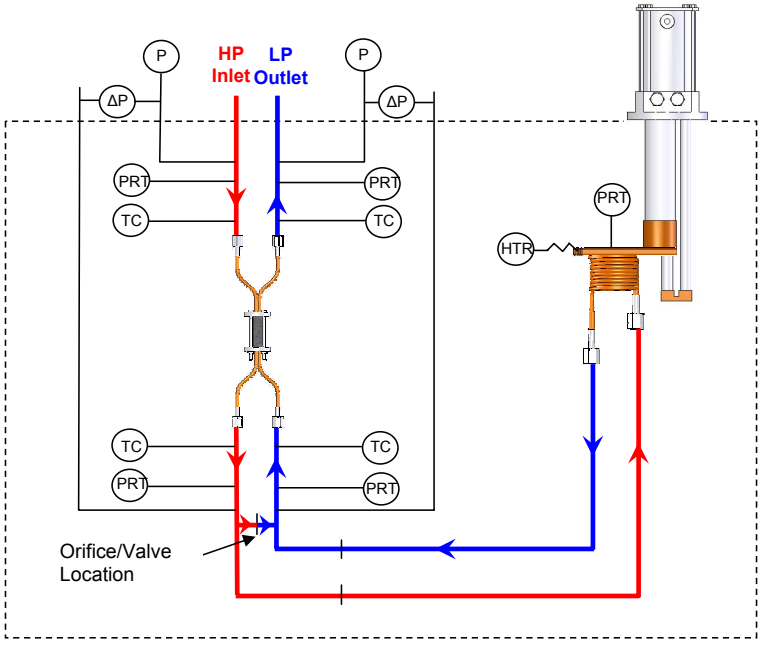

Figure 5. Flow schematic of the facility used for testing the MEMS heat exchangers

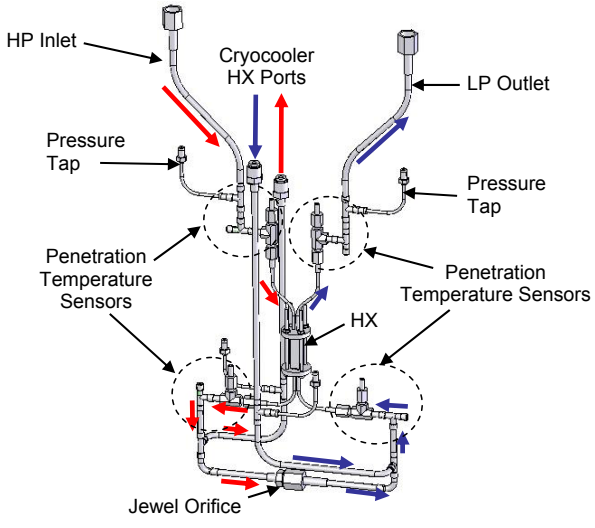

Figure 6. Geometric model of the heat exchanger instrumentation assembly

APPLIED COOLING RESULTS

The first test on the performance of the 16-die heat exchanger was an applied cooling test using helium as the working fluid. The hot inlet temperature was maintained at nominally 300 K, and the cold inlet temperature was maintained at nominally 200 K. The experimentally measured effectiveness as a function of mass flow rate is shown in the left hand plot in Fig. 7. Although the experimental effectiveness could be calculated from the PRT or thermocouple measurements, only the thermocouple measurements are shown in Fig. 7. The PRT results were not included to simplify the plots, but no information is lost because PRT and thermocouple data points were essentially identical across every experimental test condition.

There are two measured effectiveness data points for each steady state condition; one data point is based on the rate of cooling provided to the high pressure stream, and the other is based on the rate of heating provided to the low pressure stream. These quantities do not match exactly due to parasitic heat loads on the heat exchanger that cause more heat to be transferred to the low pressure stream and less heat to be removed from the high pressure stream. The parasitic heat loads were nearly constant across all data points in Fig. 7 due to the nearly constant inlet conditions. At smaller mass flow rates, the parasitic heat loads are a significant fraction of the total heat transferred between the fluid streams, which explains the larger spread between measured effectiveness at lower mass flow rates. The two methods of defining the measured effectiveness are nearly identical at higher flow rates because the parasitic heat loads are small relative to the heat transferred between the streams at higher flow rates.

A numerical model of the heat exchanger that includes estimates of the parasitic heat loads has been developed and is presented in White[7]. The numerical model was run for the same inlet conditions as the experimental data for each steady state condition. The predicted effectiveness is shown by the solid lines in Fig. 7. The numerical model is able to predict accurately the experimentally measured effectiveness over the range of mass flow rates that were tested.

An applied cooling test was also performed on the 43-die heat exchanger, and the measured results are shown in the right hand plot in Fig. 7. The 43-die heat exchanger is nearly three times as long as the 16-die heat exchanger, and thus contains nearly three times the heat transfer surface area. As expected, the 16-die effectiveness was higher across the entire range of mass flow rates due to the increased surface area and longer length, which reduces axial conduction. The numerical model is able predict the effectiveness of the longer 43-die heat exchanger with the same accuracy as for the 16-die heat exchanger.

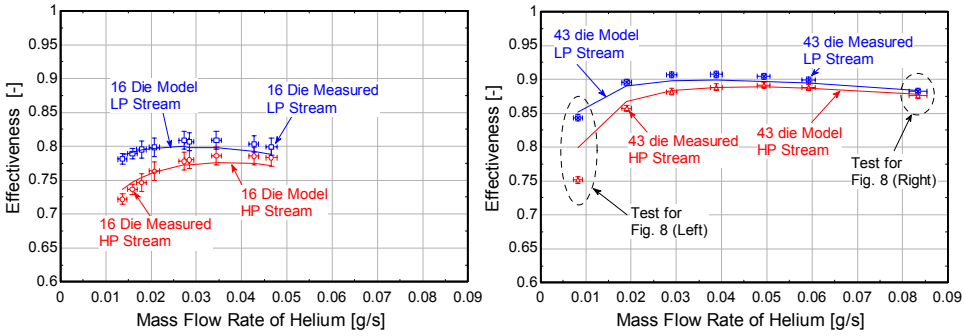

Figure 7. Experimentally measured and numerically modeled results for the applied cooling tests carried out on the 16-die heat exchanger (left) and the 43-die heat exchanger (right) using helium as the working fluid

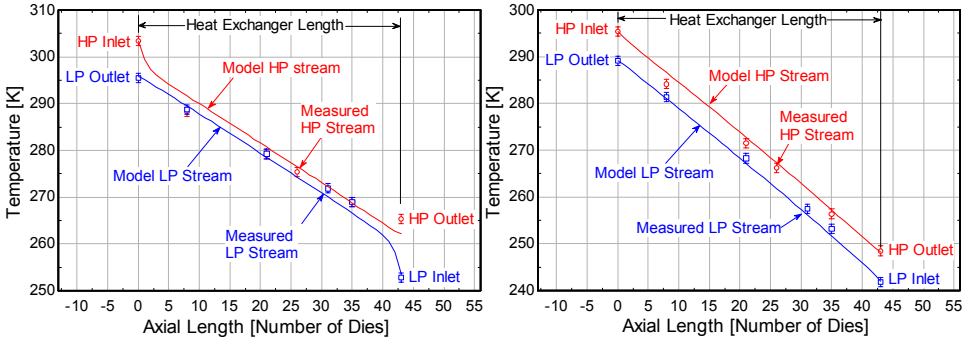

Figure 8. The experimentally measured and numerically modeled temperature distributions for the lowest (left) and highest (right) mass flow rates shown in Fig. 7 (right) for the 43-die heat exchanger.

The 43-die heat exchanger includes dies with integrated PRTs that are used to measure the internal temperature distribution. Temperature distributions within the 43-die heat exchanger were measured during the applied cooling test with helium as the working fluid, as shown in the left hand plot of Fig. 8 for the lowest mass flow rate and in the right hand plot for the highest mass flow rate. The inlet and outlet temperatures shown on the plots are measured by the penetration thermocouples, and the internal temperatures were measured by the integrated PRTs. The temperature distributions predicted by the numerical model are shown by the solid lines.

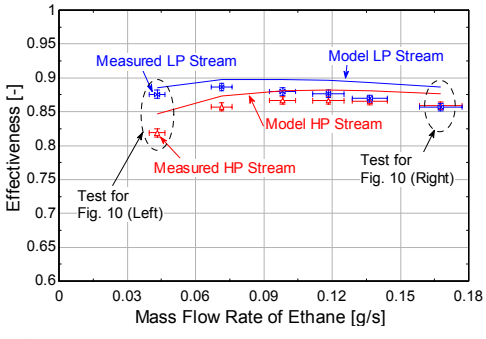

Figure 9. Experimentally measured and numerically modeled results for the applied cooling tests carried out on the 43-die heat exchanger using ethane as the working fluid

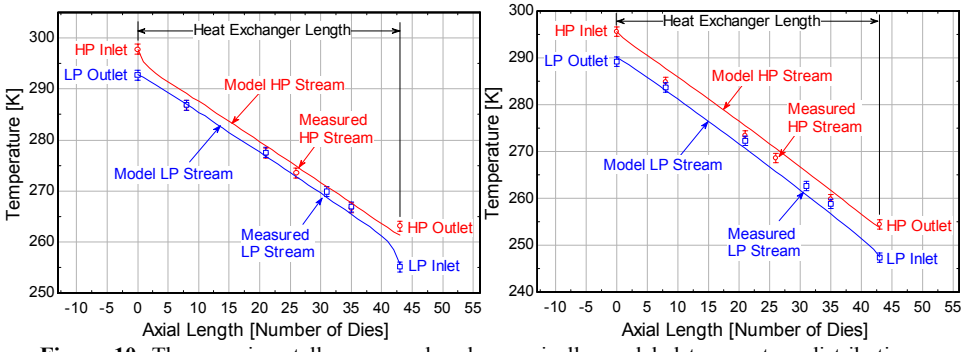

Figure 10. The experimentally measured and numerically modeled temperature distributions for the lowest (left) and highest (right) mass flow rates shown in Fig. 9 for the 43-die heat exchanger

As the mass flow rate is decreased, the number of transfer units (*NTU*) becomes higher, and therefore the average temperature difference between the two fluid streams is reduced, increasing the heat exchanger effectiveness. However, axial conduction is a major penalty at low flow rates. Analytical[8] and numerical[9] models of heat exchangers both predict abrupt "temperature jumps" at the heat exchanger ends that are related to axial conduction. These temperature jumps tend to reduce the effectiveness. As the mass flow rate increases, the *NTU* is reduced, and therefore the average temperature difference between the streams increases. However, at higher mass flow rates, the amount of heat conducted axially is small relative to the amount of heat transferred between the streams, and therefore the penalty related to axial conduction is much lower at higher flow rates. This is evident in Fig. 8 (right) by the reduction in the temperature jumps at the ends of the heat exchanger.

The experimental data and numerical model results both exhibit the trends that were expected and the measurements agree well at both high and low mass flow rates. The integrated PRTs are in better thermal contact with the silicon fins than with the fluid streams, and therefore the integrated PRT measurements should be lower than the hot fluid temperature and higher than the cold fluid temperature. In each case the measured PRT temperature (or part of the PRT uncertainty range) is between the predicted fluid temperatures.

An applied-cooling test was also carried out using ethane as the working fluid for the 43-die heat exchanger. The ethane applied-cooling test was run to verify the fidelity of the numerical model with a fluid that was more typical of the working fluid within a JT cycle. The effectiveness measurements and model predictions are shown in Fig. 9, and the temperature distributions for the smallest and largest mass flow rates are shown in Fig. 10. The model was still in good agreement with the experimental data over the range of conditions examined.

SELF COOLING RESULTS

The 43-die heat exchanger was also tested as part of a JT cycle. An actively controlled micro-valve prototype has been developed for a distributed cooling system on a satellite.[10] A photograph of the micro-valve and a geometric model with a cut-away view of the valve are shown in Fig. 11. This micro-valve had been tested at cryogenic temperatures in vacuum environments, and the prototype was thought to be suitable for use in a JT cycle. The valve is actuated by a stack of piezoelectric transducers (PZT) by a -30 V to 100 V DC signal. The valve was designed to modulate flow with only small pressure differences across the valve and therefore is not capable of completely closing at the higher pressure differences required by a JT cycle due to deflection resulting from internal pressurization. However, the valve is capable of modulating the flow and withstanding the high pressure differences and low temperatures required in a JT system.

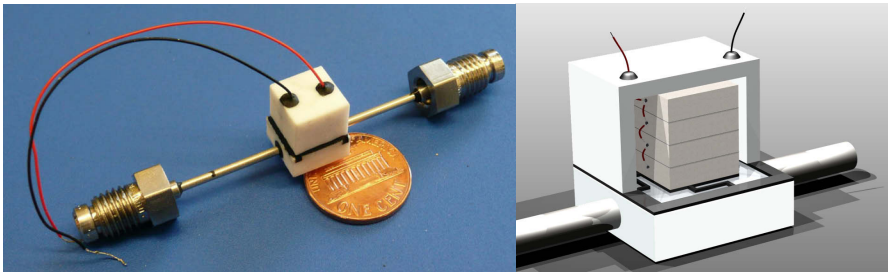

Figure 11. Photograph of the actively controlled micro-valve used for modulating the cold end temperature (left) and a cut-away view of the geometric model of the micro-valve showing PZT actuator (right).

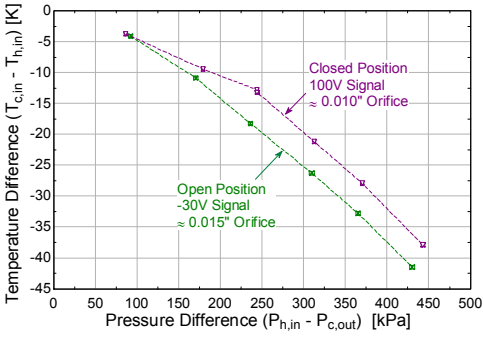

Figure 12. Temperature difference between the hot inlet and cold exit produced with the 43-die heat exchanger in self-cooling mode as a function of the pressure difference applied across the entire assembly.

The micro-valve can also be replaced with a precision jewel orifice so that the behavior of the MEMS heat exchanger can be studied without the complication of the micro-valve. The experimental results of testing the heat exchanger with the micro-valve are shown in the plot in Fig. 12. The results for the micro-valve in the fully closed position matched up very well with those obtained from testing with a 0.010 inch diameter orifice, and the results with the micro-valve in the open position matched up very well with a 0.015 inch diameter orifice. Further testing with orifices showed that the 0.015 inch diameter orifice is the optimal diameter for producing the lowest temperature over the range of pressure differences examined.

The pressure differences used during testing were limited to 450 kPa, which is only a fraction of typical pressure differences in commercial cryosurgical probes. The heat exchanger and micro-valve are constructed with brittle materials and utilized a large number of epoxied joints. The supply of heat exchanger dies and micro-valves was very limited, so breaking a MEMS component would severely hamper the experimental testing process. In addition, the test facility was not designed to destructively test components, so the failure of a component from over pressurization risks injuring personal and damaging equipment.

CONCLUSION

Progress has been made towards developing the components required for a MEMS-based cryosurgical probe. A numerical model of the heat exchanger that includes estimates of the parasitic heat loads has been developed and is able to closely predict the performance of the heat exchanger tested over a range of conditions. An actively controlled micro-valve has been demonstrated and can be used to modulate the cooling provided by the device. Temperature sensors have been integrated with the heat exchanger and provide an accurate measurement of

the temperature distribution. The spatially resolved measurement of the internal temperature distribution provides powerful verification of the design model.

A number of improvements are required before these components can be integrated into a useful cryosurgical probe. The highest priority should be to improve the die bonding technique. Stronger bonds will allow the heat exchanger to be tested at significantly higher pressures that will allow the JT cycle to reach lower temperatures and/or absorb larger heat loads. In addition, stronger bonds will eliminate or reduce the support structure, which is currently a significant source of axial conduction. Several heat exchangers have been assembled but not tested because of large internal leaks. Therefore, more robust and reliable bonding techniques will significantly improve the efficiency of the manufacturing process. Longer heat exchangers, which will have increased surface area and reduced axial conduction, will also improve the heat exchanger effectiveness.

Using optimized fluid mixtures will also improve the performance of the heat exchanger (due to the higher heat transfer coefficient associated with two-phase flow) and the JT cycle (due to the larger real gas effect associated with the multi-component mixture).[11] The numerical model is flexible, and subroutines capable of calculating mixture properties and dealing with the two-phase flow conditions can be easily integrated in order to simulate the heat exchanger performance in a mixed-gas JT cycle.

ACKNOWLEDGMENT

This work was funded by the University of Michigan through a grant from the US National Institute of Health, NIH/NINBS R21 EB003349-01.

REFERENCES

1. Dobak, J., "A Review of Cryobiology and Cryosurgery," *Advances in Cryogenic Engineering*, Vol. 43 (1998), pp. 889-896.
2. Fredrickson, K.L, *Optimization of Cryosurgical Probes for Cancer Treatment*, M.S. Thesis, University of Wisconsin-Madison (2004), http://sel.me.wisc.edu/publications/theses/theses2.html
3. Hoch, D.W. et al., "Progress Towards a Micromachined Heat Exchanger for a Cryosurgical Probe," *Cryocoolers 14*, ICC Press, Boulder, CO (2007), pp. 505-514.
4. Zhu, W. et al., "A Planar Glass/Si Micromachining Process for the Heat Exchanger in a J-T Cryosurgical Probe," *Proc. Solid State Sensors, Actuators and Microsystems*, Hilton Head (2006), pp. 51-55.
5. Zhu, W. et al., "A Perforated Plate Stacked Si/Glass Heat Exchanger with In-Situ Temperature Sensing for Joule-Thomson Coolers," *Proc. IEEE MEMS*, Tucson, Arizona, USA (2008), pp. 844-847.
6. Zhu, W. et al., "Two Approaches to Micromachining Si Heat Exchangers for Joule-Thomson Cryosurgical Probes," *Proc. IEEE MEMS*, Kobe, Japan (2007), pp. 317-320.
7. White, M.J., *Performance of a MEMS Heat Exchanger for a Cryosurgical Probe*, M.S. Thesis, University of Wisconsin-Madison (2008), http://sel.me.wisc.edu/publications/theses/theses2.html
8. Kroeger, P.G., "Performance Deterioration in High Effectiveness Heat Exchangers due to Axial Heat Conduction Effects," *Advances in Cryogenic Engineering*, Vol. 12, Plenum Press, NY (1967), pp. 363-372.
9. Nellis, G.F., "A Heat Exchanger Model that Includes Axial Conduction, Parasitic Heat Loads, and Property Variations," *Cryogenics* 43(2003), pp. 523-538.
10. Brosten, T.R., *Model and Test of an Actively Controlled Cryogenic Micro Valve*, M.S. Thesis, University of Wisconsin-Madison (2006), http://sel.me.wisc.edu/publications/theses/theses2.html
11. Skye, H.M. et. al., "Modeling and Experimental Verification of a Cascaded Mixed Gas Joule Thomson Cryoprobe," *Cryocoolers 15*, ICC Press, Boulder, CO (2009), (this proceedings).